Insights into the Interaction between Nucleoid-associated Proteins Hha and H-NS by NMR and Fluorescence Anisotropy

T. N. Cordeiro, J. García
Laboratory of Biomolecular NMR, Institut de Recerca Biomèdica-Parc Científic de Barcelona, Josep Samitier, 1-5, 08028-Barcelona, Spain

M. Pons*
Departament de Química Orgànica, Universitat de Barcelona, Martí i Franqués, 1-11, 08028-Barcelona, Spain
mpons@ub.edu

Keywords: Nucleoid-associated proteins, protein-protein interaction, chemical exchange, NMR protein recognition, fluorescence anisotropy

Abstract: *NMR and fluorescence anisotropy are both valuable tools for studying biomolecular interactions. NMR can provide structural insights at atomic resolution. Still, it can be wisely complemented by lower-resolution biophysical techniques, such as fluorescence anisotropy. In this article we report the combination of NMR and fluorescence anisotropy in establishing novel structure-function insights into the interaction between two bacterial nucleoid-associated proteins, Hha and H-NS. Hha (H-NS) complexes are known to play an important role in modulating the expression of some environmentally regulated genes that confer survival advantage in a particular growth condition.*

Resumo*: RMN e anisotropia de fluorescência são ferramentas importantes para o estudo de interações biomoleculares. Apesar da RMN proporcionar uma informação estrutural ao nível atômico, pode ser complementada por técnicas de menor resolução, como a anisotropia de fluorescência. Neste artigo é ilustrado o uso combinado de RMN com anisotropia de fluorescência no estabelecimento de novas relações função-estrutura associadas à interacção entre duas proteínas constituintes do nucleóide bacteriano, nomeadamente Hha e H-NS. Os complexos Hha(H-NS) tem um papel modulador sobre a expressão de alguns genes responsáveis pela adaptação a variações ambientais.*

Introduction

In bacteria, the chromosome is folded into a compact structure known as nucleoid. Its structural organization is determined by several factors, such as DNA super-coiling, macromolecular crowding and nucleoid-associated proteins. The combined action of these factors affects dynamically the DNA topology and compaction. Apparently there is a correlation between the way that DNA is twisted and packed, and gene transcription.[1] Nucleoid-associated proteins are specifically designed to modulate the structure of bacterial chromatin by altering the degree of compaction and levels of supercoiling.[2] Among these proteins, H-NS is known to cause DNA compaction, but more specifically, for a number of genes, it acts as a versatile transcriptional regulator; usually as a repressor.[3-5] Many of the genes affected by H-NS are important in enabling the bacteria to adapt to environmental changes, such as temperature and osmolarity variations.[6] It was suggested that H-NS affects gene transcription by interfering with the RNA polymerase ability to find access to specific genes and/or by blocking transcription elongation. The H-NS ability to generate modulatory nucleo-protein structures arises from its domain organization.[7-9] H-NS consists of an *N*-terminal protein interacting

domain, with the ability of forming homomeric and heteromeric complexes, and a *C*-terminal DNA binding domain separated by a flexible linker that is involved in the formation of high molecular weight oligomers. Truncated versions of H-NS that consist of the 64 first amino acids of *N*-terminal domain (H-NS_{64}) are capable of forming stable homodimers.[10]

The mechanisms by which H-NS acts as gene transcription modulator do not exclude the involvement of other proteins. Recent studies have led to the idea that it is highly likely that subsidiary activator/repressor proteins are required to achieve specificity in this process. Protein-protein studies have shown that the dimerization domain of H-NS (H-NS_{64}) is involved in heteromeric interaction with H-NS related proteins, such as StpA, and with members of the Hha family of proteins that lack direct DNA binding ability.[11,12] The interaction with Hha appears to be involved in modulating the expression of several environmentally regulated genes such as the *hly* operon, the *htrA* gene, or the *tra* gene from the conjugative plasmid R27.[13-15] The ability to interact with Hha-like proteins is emerging as an important theme in the mechanism of modulating the expression of specific genes as a response to environmental changes. In this paper we present an overview of NMR and fluorescence anisotropy studies on the Hha-H-NS interaction, emphasizing the complementarity of the two techniques to study protein-protein interactions.[12]

Experimental

Hha and H-NS_{64} Production

His-tagged Hha and H-NS_{64} proteins were expressed and purified as previously described.[12] Briefly, competent *E. coli* BL21 (DE3) cells were transformed with the plasmid encoding Hha and H-NS_{64}, and grown at 37ºC to an optical density at 600 nm of near 0.7. Temperature was shifted to 15ºC and protein expression induced overnight by addition of 1 and 0.5 mM IPTG respectively. Cells cultures were "pelleted" by centrifugation and then frozen at -20ºC. Hha cell pellets were resuspended in 20 mM Tris, 800 mM NaCl, 5 mM imidazole, 15 mM β-mercaptanol, pH 8.0 and lysed by sonication (6×10 s) on ice. The lysate was centrifuged, and the supernatant was collected. The soluble protein was isolated with Ni-NTA agarose (Qiagen). The resin was washed with the same buffer and the protein was eluted by a solution containing 400 mM of imidazole. For H-NS_{64}, the lysis and purification steps were carried out in the presence of 1 M NaCl, 20 mM β-mercaptanol and 0.5 mM EDTA. Gel filtration of both freshly Ni-NTA purified proteins were carried out on a Superdex 75 column in 20 mM sodium phosphate, 150 mM NaCl, 2 mM DTT, 0.01%(w/v) NaN_3, pH 7.0.

NMR experiments

All spectra were collected on a Bruker Avance 600 MHz spectrometer using 1024×128 points and 48 accumulations. Binding experiments at variable temperatures of 80-90 µM uniformly ^{15}N-labelled Hha with H-NS_{64} were performed in 20 mM sodium phosphate buffer, 150mM NaCl, 2mM DTT and 0.01%(w/v) sodium azide, pH 7.0, in the presence of 10% (v/v) ^2H_2O. NMR spectra were processed using NMRpipe. The free Hha

cross-peaks assignments were retrieved from BioMagResBank (BMRB).[16,17]

Steady-state Fluorescence experiments

Fluorescence spectra and steady-state fluorescence anisotropy measurements were carried out with an SLM-Aminco-Bowman AB2 spectro-fluorimeter using an excitation wavelength of 295 nm to selectively excite Hha Trp and an excitation bandwidth of 2nm. Emission spectra were obtained as the ratio between observed and reference signals corrected for instrument response using the apparatus correction software. Final spectra to be used for quantum yields calculation were always obtained after background fluorescence correction. Steady-state fluorescence anisotropy experiments were performed using an L-Format setup. Excitation and emission slits were adjusted at 4 nm and 8 nm respectively, for all anisotropy measurements. The anisotropy *A* was calculated according to equation 1,

$$A = \frac{\left(I_{vv} - I_{vh} \times G\right)}{I_{VV} + 2\left(I_{vh} \times G\right)} \quad \text{with} \quad G = \frac{I_{hv}}{I_{hh}} \qquad \textbf{1}$$

where I_{vv} is the fluorescence emission measured in the plane parallel to the plane of excitation and I_{vh} is the fluorescence emission measured in the plane perpendicular to the plane of excitation. *G* is a correction factor, which corrects for differential sensitivity of the detector and emission optics for vertically and horizontally polarized light. This factor was determined by comparing the fluorescence measured with the emission polarizers set to the horizontal and vertical positions after excitation with horizontally polarized light.[18] All anisotropy values were corrected for background fluorescence.

H-NS_{64} titrations were carried out at 25 ºC with freshly purified Hha and H-NS_{64} samples, in the presence of 20 mM sodium phosphate pH 7.0, 150 mM NaCl, 0.01% NaN_3 (w/v), 1 mM TCEP. The absorbance of the samples was kept below 0.05 AU to avoid fluorescence self-absorption. The sample initially contained 2 mL of 4 µM Hha and, for each point, 70 µL of a H-NS_{64} stock solution was added and incubated for 5 minutes with magnetic stirring before the measurements.

Results and Discussion

Countless biological processes involve protein-protein interactions. Identifying the structural aspects that determine the protein ability to specifically form non-covalent complexes seems to be crucial for a mechanistic description of these processes. In this context, NMR reveals to be a versatile technique for studying protein-protein interactions.[19] In addition to solving the structure of complexes, NMR data can be wisely used to map possible interface regions, as well as to estimate the affinity, stoichiometry, and specificity of binding.

HSQC NMR spectra usually present well resolved cross-peaks that can be mapped to individual protein residues. Interfaces can be identified through chemical shift perturbation, intermolecular cross-relaxation and changes in accessibility of main chain amide protons monitored through hydrogen-deuterium exchange.[20-22]

NMR experiments require relatively high concentration of isotopically labelled proteins

and complications may arise due to aggregation processes that take place at these concentrations. Low-resolution biophysical techniques can be used to derive insightful information, with less experimental demands. For instance, fluorescence-based approaches are widely used to characterise the interaction between proteins, even in a high-throughput mode.[23]

NMR Titration of ^{15}N-labelled Hha with H-NS$_{64}$

Recently, we have used an (because of the sound of "N") NMR-based approach to characterize the interaction between the bacterial nucleoid-associated proteins Hha and H-NS[12]. ^{1}H-^{15}N HSQC spectra of ^{15}N-labelled Hha were recorded in the presence of increasing amounts of unlabelled H-NS$_{64}$. It has been observed that during titration the ^{1}H-^{15}N cross-peaks become progressively broader, leading to a general decrease in intensity of the spectra. This is clearly depicted in Figure 1, which shows a superposition of HSQC spectra of free Hha and of Hha in the presence of 0.5, 1 and 3 equivalents of unlabelled H-NS$_{64}$, respectively.

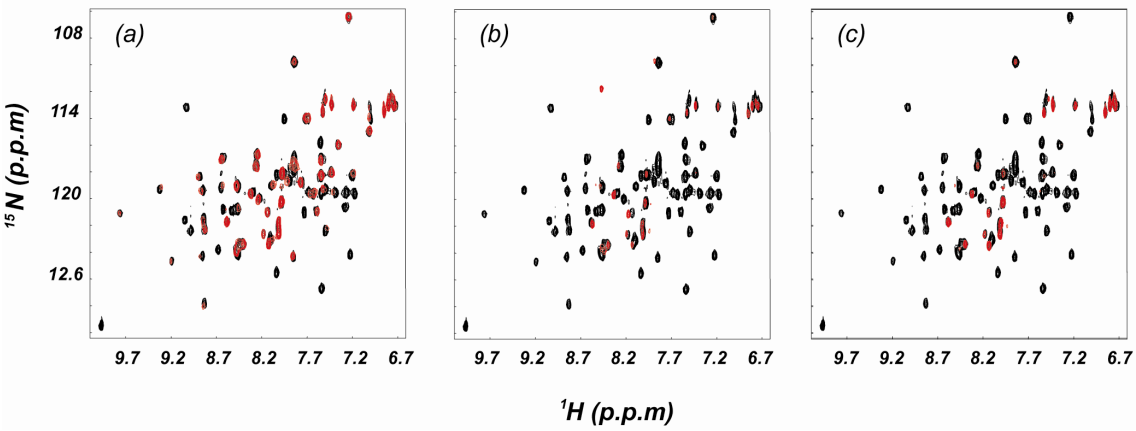

Figure 1. ^{1}H-^{15}N HSQC spectra of free Hha (black) and in the presence of 0.5 (a), 1 (b) and 3 (c) equivalents of unlabelled H-NS$_{64}$ (red).

NMR line widths are proportional to the transverse relaxation rates, R_2. These are determined by classical relaxation processes that are sensitive to fluctuations in the *ps-ns* timescales and by exchange phenomena that take place in the *ms-µs* timescales. The former are dominated by the overall tumbling of the molecule or complex, characterized by its correlation time, τ_c; large τ_c cause fast transverse relaxation, leading to broader NMR lines.

Exchange phenomena usually involve processes that stochastically transfer nuclear spins between different magnetic environments, which are linked to conformational changes or to

the complexation process itself. Globally, transverse relaxation rate is given by:

$$R_2 = R_2^* + R_{ex} \qquad \textbf{2}$$

where R_2^* is the transverse relaxation rate in the absence of chemical exchange. The transitions between the two magnetic environments, given by a certain probability, will produce a loss in the coherence reflected in the term R_{ex} of the transversal relaxation, and in turn, will contribute to additional line-broadening.

The line-broadening observed in Hha ^{1}H-^{15}N-HSQC spectra may result from the increasing of τ_c that follows complex formation and/or from chemical exchange possibilities that appear in the complex as a result of complexation.

Chemical exchange in Hha

Let us assume a two-state chemical exchange process,

$$\mathrm{A} \underset{k_-}{\overset{k_+}{\rightleftharpoons}} \mathrm{B} \qquad \textbf{3}$$

where the exchange rate constant is defined as

$$k_{ex} = k_- + k_+ \qquad \textbf{4}$$

The kinetics of the exchange process and the chemical shift differences between the exchanging sites determine different chemical exchange regimes. When the exchange frequency is lower than the frequency difference of the exchanging sites, two separate signals are observed. This corresponds to the slow exchange regime, i.e. $\frac{|\omega_A - \omega_B|}{k_{ex}} >> 1$. As exchange rate increases, the lines broaden, and coalesce when the exchange rate nears the frequency difference between sites i.e. $\frac{|\omega_A - \omega_B|}{k_{ex}} \approx 1$; this regime is referred as intermediate chemical exchange. After that, the line sharpens up until, in the limit of fast exchange, $\frac{|\omega_A - \omega_B|}{k_{ex}} << 1$, it becomes a single sharp line. In the fast regime, the extra contribution to NMR line widths caused by exchange between two states,

$$R_{ex} = p_A \cdot p_B \frac{(\omega_A - \omega_B)^2}{k_{ex}} \qquad \textbf{5}$$

depends on the sum of the forward (k_+) and reverse (k_-) rates of interconversion (k_{ex}), the frequency difference between the two sates ($\Delta\omega$) and their relative population (p_A and p_B). The frequency difference depends on the details of the exchange process, as well as the magnetic field; exchange broadening tends to be larger at higher field. The relative populations, in the case of a conformational exchange, depend on the relative energies of the two forms and the temperature, as predicated by Boltzman relationship. Maximum broadening is observed when the population of exchanging sites is the same ($p_A = p_B = 0.5$). In the case of chemical exchange due to complex formation or dissociation,

$$A + X \underset{k_-}{\overset{k_+}{\rightleftharpoons}} AX \qquad \textbf{6}$$

the population of complex and free components depend on the relative concentrations.

Exchange rates are strongly temperature sensitive. By lowering the temperature, sometimes it is possible to change from the intermediate to the slow exchange regime where signals from the exchanging sites are observed with intensities reflecting their relative populations. In the Hha-H-NS_{64} system, by lowering the temperature to 7ºC, separate signals from two species were observed and their relative intensities changed with the addition of H-NS_{64}, indicating that the two forms come from free and bound Hha. Figure 2 shows an expansion of signals from Ala46 of Hha in a series of HSQC spectra measured at 7ºC in the presence of increasing amounts of H-NS_{64}.

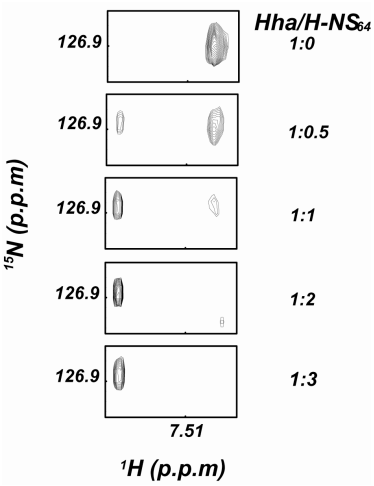

Figure 2. Expansion of signals from Ala46 of Hha in a series of HSQC spectra measured at 7ºC in the presence of increasing amounts of H-NS_{64}.

A decrease of signals from free Hha and an increase in the intensity of a new signal corresponding to the formation of a complex are clearly observed. At this temperature the viscosity is higher, and consequently, the value of τ_c for the complex becomes larger, meaning that the NMR lines would tend to get broader. However, by lowering the temperature a line-narrowing effect and duplicate signals are observed. This allows us to discard a relevant contribution of the larger τ_c of bound Hha to the line-broadening, and to consider that the broadening observed at 25ºC is caused by the chemical exchange in the intermediate regime. The decrease in temperature causes the rate of exchange to become lower than the frequency difference, and there by, separate signals are observed for the free and unbound forms. Chemical phenomena can be associated to the formation and dissociation of the complex or/and to local conformation changes. In the presence of excess of H-NS_{64} ($p_{AX} \approx 1$, $p_A \approx 0$ and $p_{AX} \cdot p_A \approx 0$), the exchange broadening due to complexation is reduced, i.e contributes least to the rate of transverse relaxation. This provides a test to distinguish between exchange caused by the complexation process itself and internal exchange phenomena. In this context, the addition of an excess of H-NS_{64} does not result in line-narrowing or increasing in intensity of signals corresponding to the formation of the complex (Figure 1). It indicates that the observed broadening corresponds not only to the dissociation and formation of the complex, but mainly to internal dynamic processes, such as conformation fluctuations. These findings could correspond to processes that were already present in the unbound protein but that are made

visible due to complex formation or new exchange possibilities appearing in the complex.

At low concentrations of H-NS_{64}, ($p_{AX} \approx 0$, $p_A \approx 1$ and $p_{AX} \cdot p_A \approx 0$), only those residues showing the largest frequency difference between exchanging sites show extensive broadening. Actually, in the presence of 0.5 equivalents of H-N_{64}, differential broadening of Hha signals is observed at 25ºC. Figure 3 shows a comparison of the intensities of the signals of the HSQC spectra measured before and after the addition of H-NS_{64}.

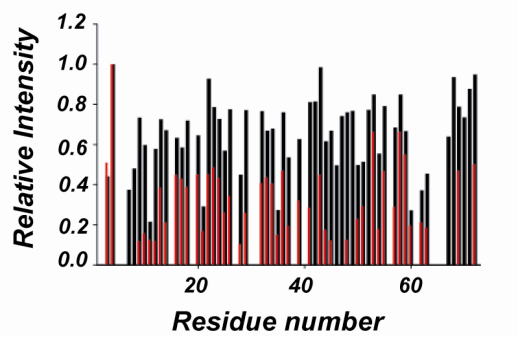

Figure 3. Normalized ^{1}H-^{15}N cross-peaks intensities of Hha in the absence (black) and in the presence (red) of 0.5 equivalents of unlabelled H-NS_{64}

Residues whose intensity is reduced by more than 75% upon the addition of 0.5 equivalents of H-NS_{64} were mapped in the structure of Hha. Surprisingly, most of the Hha residues affected by addition of H-NS_{64} have low solvent accessibility in the NMR structure published by Yee *et al.*[16] This suggests that the observed differential broadening is not only the result of direct contact of H-NS with the affected residues, but rather, the result of a conformational exchange, induced by H-NS binding, that perturbs the hydrophobic core of Hha. This is clearly illustrated in Figure 4, which compares the solvent accessibility and the position of the residues affected by the addition of H-NS_{64}; as we can see, the interaction with H-NS_{64} affects some deeply buried residues located in the interface between helices. This reinforces the idea that the observed broadening is due to a conformational exchange.

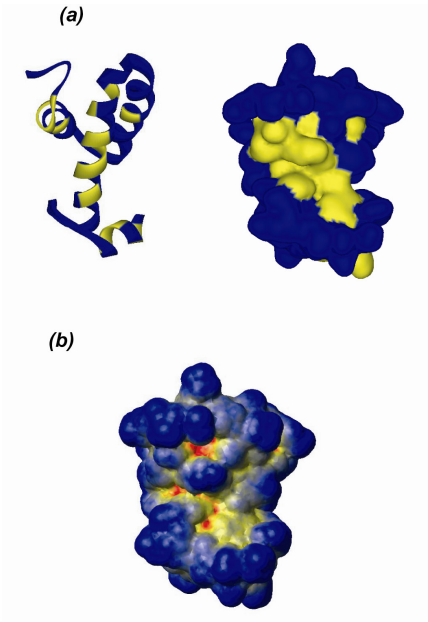

Figure 4. (a) Residues most affected by H-NS_{64} binding are highlighted on Hha structure in yellow. (b) Solvent accessibility of Hha. Residues are coloured by the percentage of solvent exposed surface: red (<5%), yellow (5 to 20%) and blue (>20%).

Although NMR data provides information about the residues most affected upon protein-protein interaction, the extensive broadening of the signals complicates the evaluation of the binding strength of Hha towards H-NS N-terminal domain. For this reason we turned to fluorescence anisotropy measurements.

Fluorescence Anisotropy as a Probe to study Hha and H-NS_{64} Interaction

Fluorescence anisotropy is a highly sensitive method for studying protein-protein interactions.[24] When plane-polarized light passes through an isotropic solution containing randomly oriented fluorophores, those molecules whose absorption transition dipole are aligned parallel to the polarization plane will be preferentially excited. In a completely rigid system, fluorescence of this subpopulation will also be polarized. However reorientation of the molecule during the life-time of the excited state (τ_F) will result in depolarization. As for NMR measurements, molecular re-orientation is described by the correlation time (τ_c),which is sensitive to molecular volume. Under steady-sate conditions, the fluorescence anisotropy of a solution can be related to the correlation time (τ_c) of the fluorophore by the Perrin equation,

$$\frac{1}{A} = \frac{1}{A_0}(1 + \frac{\tau_F}{\tau_c}) \qquad \textbf{7}$$

where A_0 is the limiting anisotropy (the anisotropy observed in the absence of any fluorophore rotation, which is determined by the angle between absorption and emission dipoles, and τ_F is the fluorescence life-time. Fluorescence anisotropy can be used to obtain hydrodynamic information concerning macromolecules and macromolecular complexes. For instance, the formation of protein-protein complexes leads to an increase in the correlation time, which will further increase the observed fluorescence anisotropy.[25] This approach has been exploited to monitor the interaction between Hha with H-NS_{64}. In contrast with Hha containing a single Trp, H-NS_{64} does not contain any Trp residue. On this basis, it seems reasonable to monitor the formation of a bio-molecular complex between Hha and H-NS_{64}, by measuring Hha fluorescence. In fact, we are in a favourable condition for monitoring the binding by a fluorescence technique since only one of the interacting species fluoresces. Here only steady-state fluorescence measurements from the single tryptophan of Hha were used to characterise this interaction, and among the fluorescence observables, fluorescence anisotropy was the most informative. Figure 5 shows the change in fluorescence anisotropy of Hha caused by the addition of H-NS_{64}. The fluorescence anisotropy of Hha increases and levels off after the addition of *circa* two equivalents of H-NS_{64} to Hha, suggesting the formation of a discrete complex (black circles). Increasing the concentration of H-NS_{64} causes a marked increase in fluorescence anisotropy (red cicles). Nevertheless, for the former experimental data a good fitting was achieved assuming the formation of a Hha/H-NS_{64} 1:2 complex with a dissociation constant of 0.45 μM^2 at 25ºC.

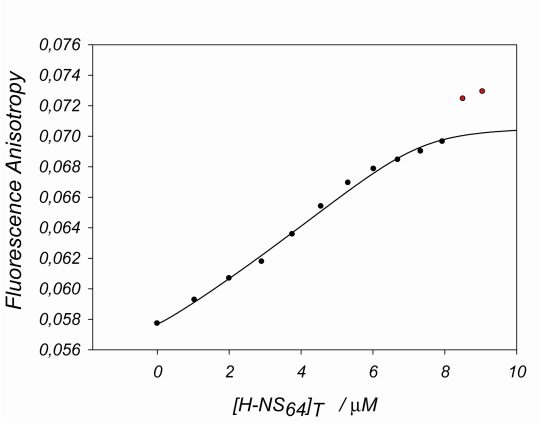

Figure 5. Fluorescence Anisotropy titration of Hha with H-NS_{64}. Black line corresponds to the theoretical binding curve

The slope of the curve of anisotropy versus H-NS_{64} concentration decreases at

approximately 2 equivalents of H-NS_{64}, but does not reach a clear plateau. So, the value of fluorescence anisotropy for the 1:2 complex (A_b) can not be directly extracted from the titration data. Instead, it is treated as an adjustable parameter in the fitting of the titration curve, along with the dissociation constant of the complex. The procedure is explained in the next subheading.

Data analysis of fluorescence anisotropy measurements

The fluorescence anisotropy of a solution containing a mixture of fluorophores(subject) is given by

$$A_i = \frac{I_{vv}^i - I_{vh}^i}{I_{vv}^i + 2I_{vh}^i} = \frac{I_{vv}^i - I_{vh}^i}{I_i} \qquad \textbf{8}$$

I_i is the fluorescence intensity for the diluted solution related to a particular fluorophore i and can be written as

$$I_i = 2.3kI_0(\lambda_E)\varepsilon_i(\lambda_E)lc_i\int_0^\infty F_i(\lambda_F)d\lambda_F \qquad \textbf{9}$$

where $\varepsilon_i(\lambda_E)$ is the molar absorption coefficient of the fluorophore i, I_0 is the intensity of the incident beam on the sample and $\varepsilon(\lambda_E)$ is the molar absorption coefficient at the excitation wavelength, λ_E; l the optical path in the sample; c_i is the concentration of the fluorophore and $F_i(\lambda_F)$ is the probability of the fluorophore emission to occur at wavelength . Its integration gives rise to the quantum yield, $\Phi_F = \int_0^\infty F(\lambda_F)d\lambda_F$. k is an instrumental factor that depends on optical configuration for observation and on the bandwidth of the monochomators.

In a fluorescence anisotropy experiment, we actually measure the components I_{vv} and I_{vh}, which are the sum of all individual components; $I_{vv} = \sum_i I_{vv}^i$ and $I_{vh} = \sum_i I_{vh}^i$. Consequently, the total fluorescence anisotropy can be defined as:

$$A = \sum_i A_i \times \frac{\varepsilon_i(\lambda_E)\Phi_F^i c_i}{\sum_i \varepsilon_i(\lambda_E)\Phi_F^i c_i} \qquad \textbf{10}$$

If all the fluorescent species have the same intrinsic fluorescence properties (i.e. the same quantum yield, Φ_F, and molar absorption coefficient, $\varepsilon(\lambda_E)$), the fraction of each is given by $f_i = \frac{I_i}{I_{total}}$, which implies that $A = \sum_i f_i \times A_i$.[18]

For the particular case of the Hha and H-NS_{64} association equilibrium, where Hha is the labelled protein (tracer species), and assuming that a sole type of complex contributes to the measured fluorescence anisotropy, the latter can be expressed as follows:

$$A = \frac{f_f \cdot A_f + f_b \cdot Q \cdot A_b}{f_f + f_b Q} \qquad \textbf{13}$$

being A_b the fluorescence anisotropy of the complex higher than the determined for free Hha (in absence of H-NS_{64}), A_f; f_f and f_b the

molar fraction of free Hha and Hha bound to H-NS_{64} respectively and $Q = \frac{\Phi_F^b \varepsilon_b(\lambda_E)}{\Phi_F^f \varepsilon_f(\lambda_E)}$.

Additionally, equation 11 can be rewritten as shown below:

$$f_b = \frac{A - A_f}{A - A_f + Q(A_b - A)} \qquad \textbf{12}$$

This equation gives us, for each data value, the fraction of bound Hha in terms of fluorescence anisotropy.

The fluorescence anisotropy data presented here were analysed assuming that the molar absorption coefficient of Hha tryptophan at the excitation wavelength does not change upon complexation. However, since fluorescence emission spectra generally are much more sensitive to the environment of the fluorophore than is light absorption, changes in quantum yield were not excluded in the data analysis. The sensitivity of fluorescence is a consequence of the relatively long time a molecule stays in an excited singlet state before deexcitation. Absorption is a process that is over in 10^{-15} seconds. On this time scale, the molecule and its environment are effectively static, and so one could assume that $\varepsilon_f(\lambda_E) \approx \varepsilon_b(\lambda_E)$. In contrast, during the 10^{-9} seconds that a singlet remains excited, all kinds of processes can occur, including protonation or deprotonation reactions, solvent relaxation, local conformational changes, and any processes coupled to translational or rotational motion. So, Q can be reduced to the ratio of the quantum yields. For diluted solutions ($A < 0.05$) this ratio becomes

$$Q = \frac{n_b^2}{n_f^2} \cdot \frac{I_b(\lambda_E, \lambda_F)}{I_f(\lambda_E, \lambda_F)} \cdot \frac{O.D_f(\lambda_E)}{O.D_b(\lambda_E)} \qquad \textbf{13}$$

where $I_f(\lambda_E, \lambda_F)$ and $I_b(\lambda_E, \lambda_F)$ are the fluorescence spectra intensity of free and bound Hha solutions, and $O.D_f(\lambda_E)$ and $O.D_b(\lambda_E)$ their optical density at the excitation wavelength, respectively. The ratio $\frac{n_b^2}{n_f^2}$ is a correction factor that accounts for changes in the refractive index. The experimental Q value in the Hha-H-NS_{64} system is nearly 1, and so this correction has minimal effects. In other systems, however, this could represent a significant source of error.

Fluorescence anisotropy data values were analysed using a model involving the putative formation of a $1:n$ complex:

$$Hha \; + \; nH\text{-}NS_{64} \rightleftharpoons Hha - (H\text{-}NS_{64})_n$$

with a dissociation constant, K_d, given by

$$K_d = \frac{[Hha]_f [H\text{-}NS_{64}]_f^{\,n}}{[Hha - (H\text{-}NS_{64})_n]} \qquad \textbf{14}$$

being $[Hha]_f$ and $[H - NS_{64}]_f$ the equilibrium concentrations of free Hha and H-NS_{64} respectively. By combining equation 14 and 16, the observed anisotropy A can be related to the known values of A_f, Q and the actual total concentrations (corrected for effects of dilution)

of Hha, $[Hha]_T$, and H-NS$_{64}$, $[H\text{-}NS_{64}]_T$, at each point by the following relationship:

$$A = \frac{A_b Q\{[H\text{-}NS_{64}]_f\}^n + A_f K_D}{K_d + Q\{[H\text{-}NS_{64}]_f\}^n} \qquad \textbf{15}$$

with

$$[H\text{-}NS_{64}]_f = [H\text{-}NS_{64}]_T - nf_b[Hha]_T$$

Since the value of A_b is experimentally unknown, the fractional saturation of Hha cannot be determined using equation 12; consequently $[H\text{-}NS_{64}]_f$ cannot be calculated. An iterative procedure was followed. The value of f_b, and therefore $[H\text{-}NS_{64}]_f$ was determined from a numerical solution of equation 16,

$$\frac{(1-f_b)\{[H\text{-}NS_{64}]_f\}^n}{f_b} - K_D = 0 \qquad \textbf{16}$$

starting from arbitrary values of K_D and n. A random search of the starting points was carried out to avoid that the calculations were trapped in local minima. The calculated $[H\text{-}NS_{64}]_f$ values and the experimental values were used to obtain a better approximation to K_D and n by fitting of equation 15 using a Marquardt-Levenberg least-squares algorithm. The procedure was repeated with the new value of K_D and n until convergence was obtained, defined in our case as $|K_{D+1} - K_D| \le 0.001$. The iterative procedure was carried out using in-house scripts written in *Mathematica* 4.0 (Wolfram Research). The procedure is illustrated in Figure 6.

The anisotropy for the complex derived from the fitting (A_b) provides an estimation of its apparent correlation time. Equation 17 relates to the correlation times of free and bound Hha molecules using the information from the ratio of anisotropies and the life time of the excited states in the two forms,

$$\tau_c^b = \frac{R\tau_c^f \tau_f^b}{\tau_c^f (1-R) + \tau_f^f} \qquad \textbf{17}$$

where $R = A_b / A_f$, τ_c^b and τ_c^f are correlation times of the free and bound forms, and τ_f^b and τ_f^f are the corresponding fluorescence lifetimes.

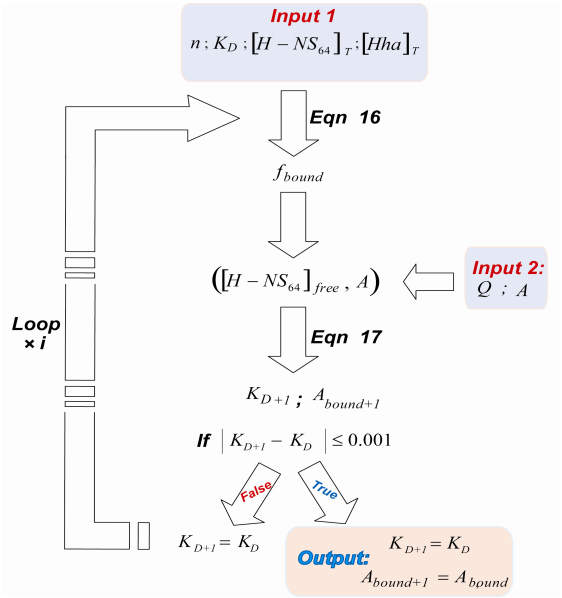

Figure 6. Schematic drawing outlining the approach used to determine the unknown binding parameters: K_D and A_b.

The fluorescence lifetimes were obtained from the relative quantum yields of free Hha and Hha in the presence of 2.5 equivalents of H-NS_{64} to Trp. The quantum yield can be written as $\Phi = \tau_F \times k_r$. Taking as a reference, the lifetime of Trp (2.6 ns at pH 7.0 and 25 ºC) and the estimation for the relative quantum yields of Hha or Hha-(H-NS_{64}) complexes, the lifetimes of Trp in Hha and Hha-(H-NS_{64}) complexes were calculated to be 2.47 and 2.35 ns respectively. The correlation time for free Hha at 25 ºC was estimated using the molecular weight of Hha, $M_w^{Hha} = 11200 \;\; Da$ and the Stokes-Einstein relationship

$$\tau_c = V_h \eta / kT \qquad \textbf{18}$$

where V_h is the hydrodynamic volume of the rotating molecule, T and η are temperature and viscosity of the solution. The hydrated specific volume of a typical protein is about 1cm^3g^{-1}. Therefore, hydrodynamic volume of a single Hha molecule will be $V_h = M_w^{Hha} / N_{Av}$, being N_{Av} the Avogadro constant . The value of viscosity for an aqueous solution at 25ºC is about 0.0094 poise.[25] The correlation time for free Hha calculated is 4.25 ns. The correlation time of the complex depends strongly on the reference correlation time assumed for free Hha. Reference values of 4 and 5 ns provide estimates of 7.6 and 11.0 ns for the correlation time of the complex using equation 8. On the other hand, the Stokes-Einstein relationship estimates that the correlation time calculated for a sphere with the mass corresponding to the molecular weight of the Hha-(H-NS_{64})$_2$ complex is 10.1 ns. This value adds force to the idea that Hha interacts with two H-NS_{64} molecules.

Conclusion

Although many structural and functional details of this system are still unsolved and demand further clarification, this paper provides the first molecular insights into the functional mechanisms by which Hha and H-NS interact. This interaction was found to involve the H-NS *N*-terminal domain (H-NS_{64}) and a conformational change of Hha. These two results were obtained by combining two biophysical techniques, NMR and fluorescence anisotropy.

Acknowledgments

This work was supported by funds from the Spanish Ministerio de Educación y Ciencia (Ramon y Cajal contract to J.G. and BIO2004-5436 to M.P.). T.N.C acknowledges the research grant SFRH/BD/21978/2005 supported by FCT, Portugal. We acknowledge the use of the NMR facilities of the Serveis Científico-Tècnics of University of Barcelona.

References

1. M. Thanbichler, S.C. Wang, L. Shapiro, *J. Cell Biochem*. **96** (2005) 506.
2. R. Dame, *Mol. Microbiol.* **56** (2005) 858.
3. R. Dame, *Nucleic Acids Res*. **28** (2000) 3504.
4. M. Yarmolinsky, *Curr. Opin. Microbiol*. **3** (2000) 138.

5. C. J. Dorman, *Nat. Rev. Microbiol.* **2** (2004) 391.
6. T. Altung, H. Ingmer, *Mol. Microbiol*. **24** (1997) 7.
7. C. J. Dorman, P. Deighan, *Curr. Opin. Gent Dev.* **13** (2003) 2179.
8. S. Rimsky, *Curr. Opin. Microbiol*. **7** (2004) 109.
9. C. J. Dorman, J.C. Hinton, A. Free, *Trends. Microbiol.* **7** (1999) 124.
10. D. Esposito, *J. Mol. Biol*. **32** (2002) 841.
11. R. M. Williams, S. Rimsky, H. Buc, *J. Bacteriol*. **178** (1996) 4335.
12. J. García, *Biochem. J.* **388** (2005) 755.
13. J. M. Nieto, *Mol. Gen. Genet*. **263** (2000) 349.
14. N. Forns, A. Juárez, C. Madrid, *FEMS microbiol. Lett*. **251** (2005) 75.
15. N. Forns, *J. Bacteriol.* **187** (2005) 3950.
16. A. Yee, *Proc.Natl. Acad.Sci. U.S.A.* **99** (2002) 1825.
17. htpp://www.bmrb.wisc.edu/ (BMRB accesión number: 5166)
18. B. Valuer, Molecular Fluorescence-Principles and Applications, Wiley-VCH, Weinheim, 2002.
19. E.R. Zuiderweg, *Biochemistry* **41** (2002) 1.
20. M. P. Foster, *J. Biomol. NMR* **12** (1998) 51.
21. H. Takahashi, *Nat. Struct. Biol.* **7** (2000) 220.
22. Y. Paterson, S.W. Englander, H. Roder, *Science* **249** (1990) 755.
23. Y. Yan, G. Marriot, *Curr. Opin. Chem. Biol*. **7** (2003) 635.
24. D.M. Jameson, W.H. Sawyer, *Meth. Enzymol.* **246** (1995) 283.
25. R. C. Cantor, P. R. Schimmel Biophysical Chemistry: Part II: Techniques for the study of biological structure and function, Freeman W. H. and Co., San Francisco, 1980.